Available online at www.sciencedirect.com
ScienceDirect
Journal of Power Sources 159 (2006) 1365–1369
JOURNAL OF POWER SOURCES
www.elsevier.com/locate/jpowsour

Lithiated manganese oxide $Li_{0.33}MnO_2$ as an electrode material for lithium batteries

C.M. Julien [a], B. Banov [b], A. Momchilov [b], K. Zaghib [c,*]

[a] *Institut des Nano-Sciences de Paris, CNRS-UMR 7588, Université Pierre et Marie Curie, Campus Boucicaut, 140 rue de Lourmel, 75015 Paris, France*
[b] *Institute of Electrochemical and Energy Systems, Bulgarian Academy of Sciences, Acad. G. Bonchev Str., Block 10, 1113 Sofia, Bulgaria*
[c] *Institut de Recherches d'Hydro-Québec, 1800 Boul. Lionel-Boulet, Varennes, Que., Canada J3X 1S1*

Received 8 November 2005; received in revised form 15 December 2005; accepted 15 December 2005
Available online 7 February 2006

Abstract

$Li_{0.33}MnO_2$ was prepared by solid-state reaction of CMD oxide and a lithium salt. The structure was studied by X-ray diffraction and Raman scattering during electrochemical discharging. The possibility of application as a positive electrode in rechargeable lithium batteries was investigated. The electrochemical properties of Li//$Li_{0.33}MnO_2$ cells were studied as a function of temperature in the range 25–55 °C. The electrode material delivers an initial capacity of 194 mAh g^{-1} and shows good reversibility at room temperature. Finally, the lithium insertion mechanism was examined by the determination of the ion kinetics.

Keywords: Lithium batteries; Manganese dioxides; Structural properties; Diffusion coefficient

1. Introduction

During the last decade, manganese-based oxides have been the most investigated materials as positive electrodes for secondary lithium batteries [1]. They provide safety, low-cost, low toxicity and high performance, so that a commercial battery based on such compounds is viable. Many kinds of porous manganese oxide crystals with tunnel and layered structures have been reported [2]. Indeed, Tadiran has commercialized a Li//Li_xMnO_2 rechargeable cell, which has a unique safety system. It is based on an electrolyte which polymerizes with rise in temperature to prevents further exothermic reaction.

The backbone of the structure consists on a network of corner-shared and/or edge-shared MoO_6 octahedra. It has been reported, however, that the chemically grown manganese dioxide (CMD) has a poor long term cyclability [3]. Several workers have studied the structural stability and the electrochemical properties of chemically lithiated MnO_2-based compounds [3–8]. In order to improve the rechargeability of MnO_2, different phases have been synthesized. A lithium-containing manganese dioxide as a composite dimensional manganese oxide (CDMO) contains domains of β–γ-MnO_2 and the rock-salt structure Li_2MnO_3 [9]. An intergrowth structure, containing domains of a lithiated γ-MnO_2 phase has been prepared by the acid digestion of the spinel phase under carefully controlled conditions [10]. The lithiated $Li_{0.33}MnO_2$ phase has been obtained by heat treatment of a mixture of LiOH-MnO_2 and $LiNO_3$-MnO_2 at low temperature and behaved as a 3-V electrode material in liquid–electrolyte lithium batteries. This compound delivered a rechargeable capacity of 180 mAh g^{-1} with a flat potential of 2.9 V versus Li^0/Li^+ [9–15].

In this paper, we report the electrochemical and structural properties of the $Li_{0.33}MnO_2$ electrode materials prepared by solid-state reaction of CMD and lithium salt. The morphology and structure are studied by scanning electron microscopy (SEM), X-ray diffractometry (XRD) and Raman scattering (RS) spectroscopy. The possibility of application as a positive electrode in rechargeable lithium batteries was investigated as a function of the cell temperature.

2. Experimental

The lithiated MnO_2 samples were prepared by the classical solid-state reaction (SSR) of CMD oxide and $LiNO_3$ as the

* Corresponding author. Tel.: +1 450 652 8019; fax: +1 450 652 8424.
E-mail address: zaghib.karim@ireq.ca (K. Zaghib).

0378-7753/$ – see front matter © 2006 Elsevier B.V. All rights reserved.
doi:10.1016/j.jpowsour.2005.12.011

lithiated agent, according to the method conditions of synthesis described elsewhere [7]. A final temperature of pre-treatment in the range 350–450 °C was chosen. Applying a multi-step technique, the starting material (CMD Faradizer M) was thermally pre-treated at 350 °C for 12 h without the lithiating agent to remove the adsorbed and chemically bound water. An intimate mixture of the precursor and lithium salt was reacted in a Pt crucible at 250 °C for 24 h, at 350 °C for 24 h, and finally fired at 450 °C for 8 h.

The particle morphology of the $Li_{0.33}MnO_2$ powders was examined with a scanning electron microscope (SEM, Philips XL30). The specific surface area was measured by the BET method (Nova 2000). Phase identification was carried out by XRD using a Philips X'Pert PRO MRD (PW3050) diffractometer equipped with a Cu anticathode (Cu Kα radiation $\gamma = 1.54056$ Å) at room temperature. RS spectra of the samples were collected with a double monochromator (Jobin–Yvon model U1000) using the 514.5 mn laser line from a Spectra-Physics 2020 Ar-ion laser. The electrochemical properties of the product were tested at room temperature in cells with metallic lithium as the anode. Measurements were carried out following the experimental procedure previously described [16] using Teflon laboratory-cell hardware and the Mac-Pile system. Quasi open-circuit voltage curves were recorded using a current pulse of 0.14 mA cm^{-2} applied for 1 h followed by a relaxation period of 0.5–1.0 h, to record the transient voltage for the determination of chemical diffusion coefficients of Li^+ ions in the $Li_{0.33}MnO_2$ electrode.

3. Results and discussion

The synthesized product has the chemical formula $Li_{0.33}MnO_2$ with a specific surface area of 28–32 $m^2\,g^{-1}$ estimated from BET measurements. The surface morphology and texture as well as the particle sizes of $Li_{0.33}MnO_2$ specimens were observed by SEM which show data consistent with the BET measurements. Fig. 1(a and b) shows the typical SEM pictures recorded at various magnifications of the $Li_{0.33}MnO_2$ powders synthesized by solid-state reaction. It can be seen that the small particles in the sample are highly regular. Both the size and the form of the particles is even. Most of the particles have a regular shape with roundness of the edges, and their dimensions are submicron, i.e. the grain size average is around 600 nm.

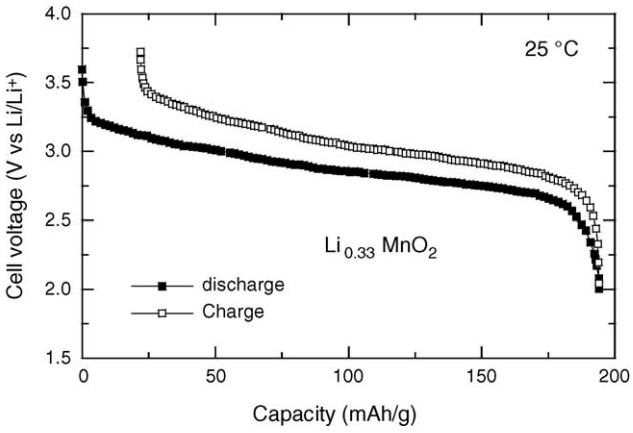

Fig. 2. The first discharge–charge curves of Li//$Li_{0.33}MnO_2$ cells in the voltage range 4.0–1.5 V vs. Li^0/Li^+. Measurements were carried out at 25 °C.

The marked decrease in the particle size of $Li_{0.33}MnO_2$, compared with the CMD precursor is then unequivocally correlated with the kinetics of grain formation using the SSR synthesis as low as 450 °C which favours this tendency for small grains.

Fig. 2 shows the first discharge–charge curves for the Li//$Li_{0.33+x}MnO_2$ cells in the voltage range 4.0–1.5 V versus Li^0/Li^+ at a current density 0.14 mA cm^{-2}. Measurements were carried out at 25 °C. For the first discharge–charge process, the voltage profile occurs with an S-shape that indicates the formation of a single-phase $Li_{0.33+x}MnO_2$. This electrode material has an initial capacity of 194 mAh g^{-1}, corresponding to 0.62Li/Mn intercalating into the $Li_{0.33}MnO_2$ host lattice. The capacity observed here is in good agreement with the theoretical gravimetric capacity of 201 mAh g^{-1} based on the following reaction

$$Li_{0.33+x}MnO_2 + 0.67Li^+ + 0.67e^- \rightleftarrows LiMnO_2. \quad (1)$$

Since the reduction process of $Li_{0.33}MnO_2$ is reversible, the construction of rechargeable cells is possible. Satisfactory charge–discharge efficiency and storage capability are other favorable features of this cell. Upon lithiation of the $Li_{0.33+x}MnO_2$, the electronic conductivity increases slightly from 1×10^{-4} S cm^{-1} for $x = 0$ to ca. 5×10^{-3} S cm^{-1} for $x = 0.55$. Fig. 3 shows the incremental capacity of the Li//$Li_{0.33+x}MnO_2$ cells derived from the titration curve at 25 °C.

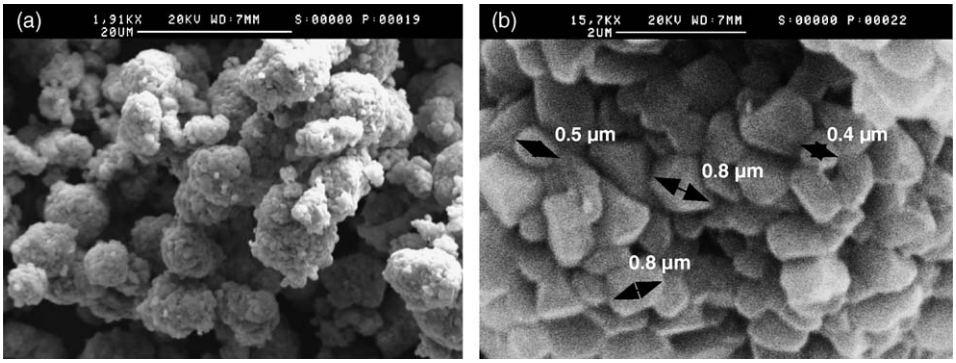

Fig. 1. SEM images at various magnifications of the $Li_{0.33}MnO_2$ synthesized by solid-state reaction.

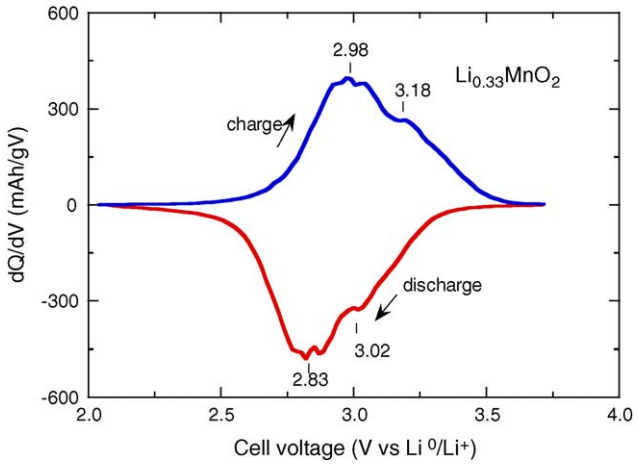

Fig. 3. Incremental capacity of the Li//$Li_{0.33+x}MnO_2$ cells derived from the titration curve at 25 °C. Reduction peaks appeared at 3.02 and 2.83 V while oxidation peaks occurred at 2.98 and 3.18 V.

Reduction peaks appeared at 3.02 and 2.83 V, while oxidation peaks occurred at 2.98 and 3.18 V.

Fig. 4a and b presents the temperature dependence of the discharge–charge curves. It is shown that the Li//$Li_{0.33}MnO_2$ cells can operate efficiently at temperatures of 40 and 55 °C at about 190 mAh g^{-1} or less with an operating voltage in the range 1.5–3.8 V. The electrochemical profile of cells heated at 40 and

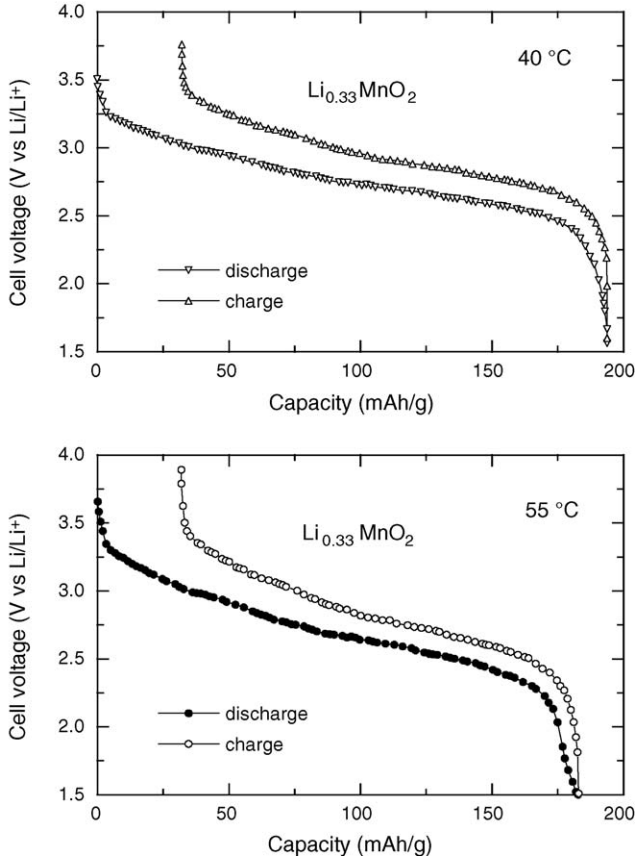

Fig. 4. Temperature dependence of the first discharge–charge curves of Li//$Li_{0.33}MnO_2$ cells in the voltage range 4.0–1.5 V vs. Li^0/Li^+. Measurements were carried out at 40 and 55 °C.

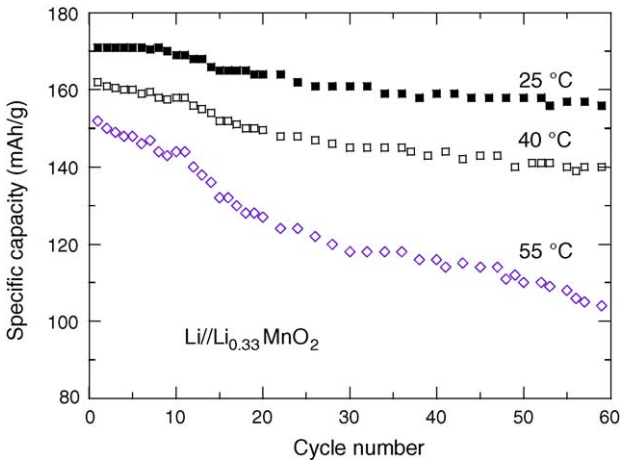

Fig. 5. Cycling behaviour of the Li//$Li_{0.33+x}MnO_2$ cell as a function of the temperature.

55 °C shows a slight decrease of the initial capacity but a decline of the average voltage is observed. In the case of Li//$Li_{0.33}MnO_2$ operating at 55 °C, the average cell voltage is about 7% less than for the cell operating at 25 °C. Fig. 5 displays the cycling behaviour of the Li//$Li_{0.33+x}MnO_2$ cell as a function of the temperature. These electrochemical tests were carried out in Li/1 M $LiClO_4$ in EC-DEC/$Li_{0.33}MnO_2$ cells. The comparative diagram for cycle behavior shows that for a temperature rising to 55 °C, the capacity retention decreases by 50% after the 60th cycle. This phenomenon is attributed to the phase transformation from monoclinic $Li_{0.33}MnO_2$ to a $LiMn_2O_4$ spinel. This structural destabilization occurring during electrochemical cycling is well known for $LiMnO_2$ [16,17]. The above characteristics are used to calculate the thermodynamics of the Li activity in $Li_{0.33+x}MnO_2$. The open-circuit voltage, E, of a lithium cell can be related to the thermodynamic free energy, ΔG_{Li}, of the electrochemical reaction taking place as

$$\Delta G_{Li}(x, T) = nFE(x, T) = \Delta H_{Li}(x, T) - T\Delta S_{Li}(x, T). \quad (2)$$

Combining this equation with the classical relationship of thermodynamics at constant pressure $\partial\Delta G/\partial T = -\Delta S$, one obtains the expression for the variation of entropy

$$\Delta S_{Li}(x, T) = -nF\frac{\partial E}{\partial T} \quad (3)$$

For low lithium contents, $x \sim 0.1$, high value of entropy is found reflecting the random distribution of Li ions, i.e. a high mobility in the host lattice. This is consistent with a system exhibiting a large value for the ion–ion interaction factor. Beyond $x = 0.3$ from an initial value of 1.27 kJ mol^{-1} K^{-1}, $\Delta S_{Li}(x,T)$ slowly increases up to $x = 0.62$.

To understand the electrochemical features of the $Li_{0.33+x}MnO_2$ positive electrode, structural properties were measured as a function of state-of-discharge (SOD) using XRD and RS experiments. Fig. 6 presents the XRD patterns of electrochemically intercalated $Li_{0.33+x}MnO_2$ materials. The crystal structure of $Li_{0.33}MnO_2$ obtained by heat-treatment of a γ-MnO_2 and $LiNO_3$ mixture belongs to the space group $C2/m$ with the lattice parameters $a = 14.08$ Å, $b = 2.81$ Å and

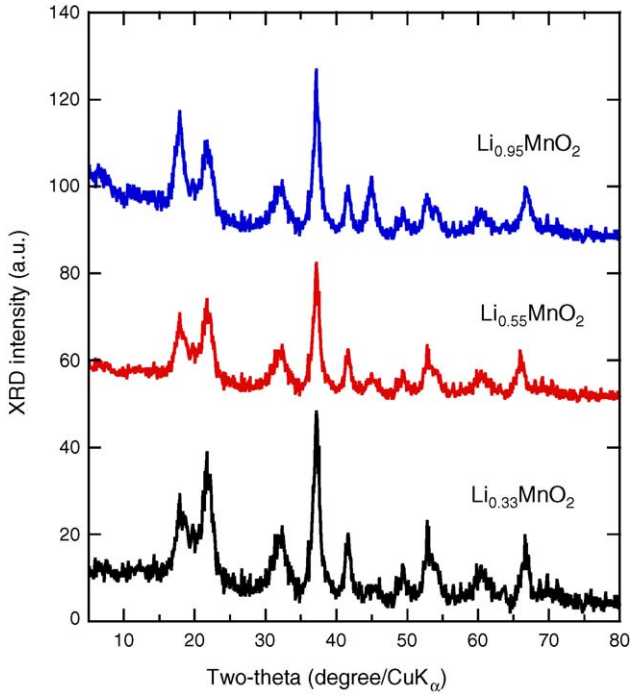

Fig. 6. XRD patterns of electrochemically intercalated $Li_{0.33+x}MnO_2$ compounds. New diffraction peaks are growing at $2\theta = 18$ and 45° upon Li insertion.

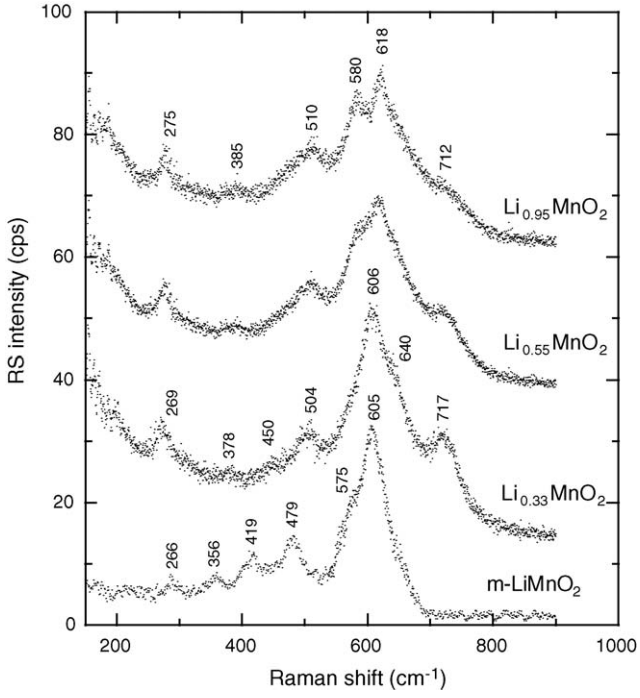

Fig. 7. Raman scattering spectra of lithiated $Li_{0.33+x}MnO_2$ compounds. The stretching modes in the region 600–650 cm^{-1} are shifted toward the low wavenumber side upon Li insertion.

$c = 4.47$ Å. The crystal lattice consists of the arrangement of MnO_6 octahedra with the hexagonal close packed oxygen lattice providing two different sites for Mn cations, which leads to an open framework for easy Li-ion motion. The results shown in Fig. 6, i.e. shape and positions of the Bragg lines, indicate that the framework structure of $Li_{0.33}MnO_2$ is almost unchanged during the discharge reaction up to 0.62Li/Mn. However, one can observe the appearance of new diffraction peaks at $2\theta = 18$ and 45° upon Li insertion. This is the result of a continuous structure reorganization, which indicates complete reversibility of the insertion–extraction process for $Li_{0.33}MnO_2$ material in the potential range 3.8–1.5 V.

Fig. 7 shows the RS spectra of the $LiMnO_2$ monoclinic phase and the lithiated $Li_{0.33+x}MnO_2$ compounds. For lithiated $Li_{0.33+x}MnO_2$ electrodes, the stretching modes in the region 600–650 cm^{-1} are shifted toward the low wavenumber side upon Li insertion. The two dominant Raman bands of $Li_{0.33}MnO_2$ at 606 and 640 cm^{-1} are attributed to the stretching modes of MnO_6 octahedra and correspond to the A_g species in the C_{2h}^3 spectroscopic symmetry. The high wavenumber peak at 718 cm^{-1} belongs to the B_g symmetry. The bands at 378, 450 and 504 cm^{-1} are assigned to the bending modes of the O–Mn–O bonds. The low wavenumber band located at 269 cm^{-1} is due to the vibrations of Li ions in the octahedral cage. The net effect of the Li-ion incorporation into the tunnels of the $Li_{0.33}MnO_2$ lattice results in a small modification of the Raman spectrum. We observe a shift of the stretching vibrations toward the lower wavenumber side due to the reduction of Mn ions. The lowering of the oxidation state of manganese from Mn^{4+} to Mn^{3+} induces an increase in the elementary unit cell, which results in a decrease of the vibrational mode frequencies that is inherent in the presence of Mn^{3+} ions. These spectral features are also observed in the RS spectrum of the $LiMnO_2$ monoclinic phase. For this compound, the stretching modes of the MnO_6 octahedra occur at 575 and 605 cm^{-1} due to the greater Mn–O distances. Comparison of the RS spectra leads the conclusion that the Li^+ ions are inserted into the octahedral voids of the $Li_{0.3''}MnO_2$ host lattice.

The diffusion kinetics of the Li^+ insertion–extraction process directly controls the rate of discharge and charge of the cells. The chemical diffusion coefficient of Li^+ ions, D_{Li}^*, was determined using the GITT method [18]. An estimate of the chemical diffusion coefficient of Li^+ has been elaborated analysing the semi-infinite diffusion part of the transient voltage

$$D_{Li}^* = \frac{4}{\pi}\left(\frac{V_m}{FSZ}\right)^2 \left[I_0 \left(\frac{\partial E}{\partial x}\right) \left(\frac{\partial E}{\partial \sqrt{t}}\right)^{-1} \right]^2 \quad (4)$$

where V_m is the molar volume, S the geometric apparent area of the electrode (estimated from BET data), I_0 the current supplied, F the Faraday constant, $(\partial E/\partial x)$ the slope of the coulometric titration curve, while $\partial E/\partial\sqrt{t}$ is the slope of the short-time transient voltage change. At any composition, Eq. (4) is valid for times shorter than the diffusion time $\tau \ll L^2/D_{Li}^*$ [18].

Fig. 8 shows the evolution of D_{Li}^* for the $Li_{0.33+x}MnO_2$ electrode as a function of the degree of Li insertion. The graph (dx/dV) versus x obtained from the titration curve is also shown (open circles). The chemical diffusion coefficients of Li ions in the $Li_{0.33+x}MnO_2$ electrode depend on x. D_{Li}^* is found to range from 6×10^{-11} to 3×10^{-11} $cm^2\,s^{-1}$ for $Li_{0.33}MnO_2$ and $Li_{0.95}MnO_2$, respectively, with a minimum value at ca. 3×10^{-12} $cm^2\,s^{-1}$ for $x \approx 0.75$. This minimum

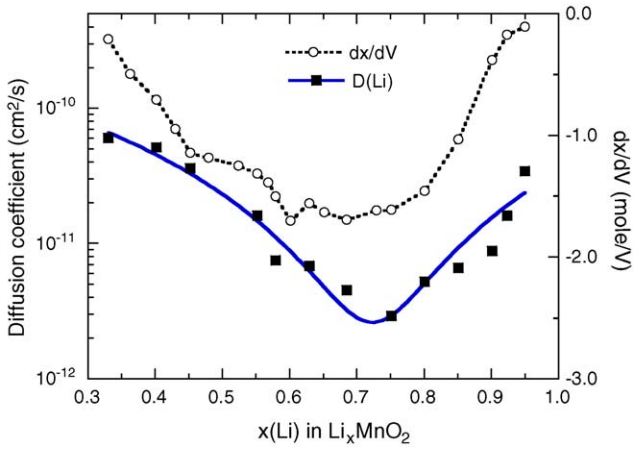

Fig. 8. Chemical diffusion coefficient of Li^+ ions in the $Li_{0.33+x}MnO_2$ electrode as a function of the degree of Li insertion. The graph (dx/dV) vs. x obtained from the titration curve is also shown (open circles).

is in correspondence of the peak of the differential capacity. The minimum in D^*_{Li} was predicted by the model for strong attractive interactions between the insertion species and the host matrix [19]. The Li mobility is shown to slightly decrease upon subsequent discharge–charge cycles due to irreversible structural and morphological changes of the host matrix. The value of D^*_{Li} are in close agreement with other oxygen-packed frameworks such as $LiMoO_3$ [20].

4. Conclusions

The electrochemical properties of the $Li_{0.33}MnO_2$ electrode materials, prepared by a solid-state reaction of CMD and lithium salts, has been studied. A Faradaic yield 0.62Li/Mn was achieved upon discharge, leading to a capacity of 194 mAh g^{-1}. The Li//$Li_{0.33}MnO_2$ electrodes have been tested at different temperatures in the range 25–55 °C. At 55 °C, the cell displays a smaller capacity retention and a slight decrease of the average cell potential. X-ray diffraction and Raman spectroscopy show that the host lattice remains intact upon Li^+ ion insertion and extraction. The chemical diffusion coefficients of the Li ions varies in the range 6×10^{-11} to 3×10^{-12} cm^2 s^{-1}.

References

[1] D. Guyomard, in: T. Osaka, M. Datta (Eds.), Energy Storage Systems for Electronics, Gordon and Breach Sci. Publ., Amsterdam, 2000, p. 253.
[2] Q. Feng, H. Kanoh, K. Ooi, J. Mater. Chem. 9 (1999) 319.
[3] G. Pistoia, J. Electrochem. Soc. 129 (1982) 1861.
[4] M. Yoshio, S. Inoue, M. Hyakutake, G. Piao, H. Nakamura, J. Power Sources 34 (1991) 147.
[5] L. Li, G. Pistoia, Solid State Ionics 47 (1991) 231.
[6] L. Li, G. Pistoia, Solid State Ionics 47 (1991) 241.
[7] B. Banov, A. Momchilov, A. Trifonova, B. Puresheva, J. Power Sources 81–82 (1999) 562.
[8] T. Nohma, T. Saito, N. Furukawa, H. Ikada, J. Power Sources 26 (1989) 389.
[9] T. Ohzuku, M. Kitagawa, T. Hirai, J. Electrochem. Soc. 136 (1989) 3169.
[10] M.M. Thackeray, M.H. Rossouw, R.J. Gummow, D.C. Liles, K. Pearce, A. de Kock, W.I.F. David, S. Hull, Electrochim. Acta 38 (1993) 1259.
[11] M. Yoshio, H. Nakamura, H. Nogushi, Prog. Batteries Sol. Cells 9 (1990) 205.
[12] M. Yoshio, H. Nakamura, Y. Xia, Electrochim. Acta 45 (1999) 273.
[13] B. Banov, A. Momchilov, M. Massot, C.M. Julien, Mater. Sci. Eng. B 100 (2003) 87.
[14] M.M. Thackeray, M.H. Rossouw, A. de Kock, A.P. de la Harp, R.J. Gummow, K. Pearce, D.C. Liles, J. Power Sources 43–44 (1993) 289.
[15] E. Levi, E. Zinigrad, H. Teller, M.D. Levi, D. Aurbach, J. Electrochem. Soc. 145 (1998) 3440.
[16] C. Julien, S. Ziolkiewicz, M. Lemal, M. Massot, J. Mater. Chem. 11 (2001) 1837;
G. Vitins, K. West, J. Electrochem. Soc. 144 (1997) 2587.
[17] Y.-I. Jang, B. Huang, Y.-M. Chiang, D.R. Sadoway, Electrochem. Solid-State Lett. 1 (1998) 13.
[18] W. Weppner, R.A. Huggins, J. Electrochem. Soc. 124 (1977) 1569.
[19] T. Ohzuku, K. Nakura, T. Aoki, Electrochim. Acta 45 (1999) 151.
[20] B. Yebka, C. Julien, Solid State Ionics 90 (1996) 141.